

Article

Control Landscape of Measurement-Assisted Transition Probability for a Three-Level Quantum System with Dynamical Symmetry

Maria Elovenkova and Alexander Pechen * 

Department of Mathematical Methods for Quantum Technologies, Steklov Mathematical Institute of Russian Academy of Sciences, 8 Gubkina Str., Moscow 119991, Russia; elovenkova.m@phystech.edu

* Correspondence: apechen@gmail.com

Abstract: Quantum systems with dynamical symmetries have conserved quantities that are preserved under coherent control. Therefore, such systems cannot be completely controlled by means of only coherent control. In particular, for such systems, the maximum transition probability between some pairs of states over all coherent controls can be less than one. However, incoherent control can break this dynamical symmetry and increase the maximum attainable transition probability. The simplest example of such a situation occurs in a three-level quantum system with dynamical symmetry, for which the maximum probability of transition between the ground and intermediate states using only coherent control is $1/2$, whereas it is about 0.687 using coherent control assisted by incoherent control implemented through the non-selective measurement of the ground state, as was previously analytically computed. In this work, we study and completely characterize all critical points of the kinematic quantum control landscape for this measurement-assisted transition probability, which is considered as a function of the kinematic control parameters (Euler angles). The measurement-driven control used in this work is different from both quantum feedback and Zeno-type control. We show that all critical points are global maxima, global minima, saddle points or second-order traps. For comparison, we study the transition probability between the ground and highest excited states, as well as the case when both these transition probabilities are assisted by incoherent control implemented through the measurement of the intermediate state.



Citation: Elovenkova, M.; Pechen, A. Control Landscape of Measurement-Assisted Transition Probability for a Three-Level Quantum System with Dynamical Symmetry. *Quantum Rep.* **2023**, *5*, 526–545. <https://doi.org/10.3390/quantum5030035>

Academic Editor: Walter E. Lawrence

Received: 5 May 2023

Revised: 30 June 2023

Accepted: 4 July 2023

Published: 13 July 2023



Copyright: © 2023 by the authors. Licensee MDPI, Basel, Switzerland. This article is an open access article distributed under the terms and conditions of the Creative Commons Attribution (CC BY) license (<https://creativecommons.org/licenses/by/4.0/>).

Keywords: quantum measurement; measurement-assisted quantum control; quantum control landscape; dynamical symmetry; second-order trap

1. Introduction

Quantum control attracts high interest due to fundamental reasons related to the ability to manipulate quantum systems and due to various existing and prospective applications in quantum technologies [1]. Coherent control is realized by lasers or an electromagnetic field [2–4]. Incoherent control can be realized by various forms of the environment. One particular form of incoherent control is control using the *back-action of non-selective quantum measurements*, either projective or continuous. The general formulation for assisting the coherent control of quantum systems using the back-action of non-selective quantum measurements was developed in [5]. Various incoherent control strategies using the back-action of quantum measurements have been applied to many problems, such as enhancing the controllability of systems with dynamical symmetry [6], developing incoherent control schemes for quantum systems with wavefunction-controllable subspaces [7], using measurements to enhance controllability [8], manipulating a qubit [9], incoherently controlling retinal isomerization in rhodopsin [10], controlling transitions in the Landau–Zener system [11], modifying the decay rates of excited states in open quantum systems [12], inducing Boolean dynamics for open quantum networks [13], steering quantum states by using the sequences of weak blind measurements [14], incoherently controlling a qubit using the quantum

Zeno effect [15], applying decoherence-assisted optimal quantum state preparation [16], building quantum-feedback-like models of photosynthesis [17], controlling quantum state transfer based on the optimal measurement [18], etc. The energy-measurement-induced quantum damping of position for an atom bouncing on a reflecting surface in the presence of a homogeneous gravitational field was investigated [19]. The measurement-induced decoherence of trapped ions prepared in a nonclassical motional state was shown to inhibit the internal population dynamics and damp the vibrational motion [20]. The mapping of an unknown mixed quantum state onto a known pure state using the sequential measurements of two noncommuting observables only and without the use of unitary transformations was studied [21]. Zeno-type effects in a superconducting qubit in the presence of structured noise baths and variable measurement rates were used to suppress and accelerate qubit decay [22]. Quantum measurements were used to control weak values in the Cheshire Cat effect in open quantum systems [23]. A quantum clock driven by entropy reduction through measurement was proposed [24]. The Zeno effect was used to demonstrate universal control between non-interacting qubits [25] and generate a multi-qubit entangling Zeno gate [26]. A measurement-based estimator scheme for continuous quantum error correction was proposed [27]. Steering a two-level system using weak measurements in addition to the system Hamiltonian was shown to allow the targeting of any pure or mixed state [14]. Stroboscopic driving combined with repeated measurement-like interactions with an external spectator system was applied for optimal quantum state preparation [16]. A measurement-based feedback approach with reinforcement learning exploiting the non-linearity of weak measurements with coherent driving was proposed to prepare cavity Fock state superpositions [28]. Measurement-based control was applied to find the minimum energy eigenstate of a given energy function [29]. The control of two-level systems by using positive unital maps associated with quantum Lotka–Volterra operators was considered [30]. Projective quantum measurement induces the collapse of the wavefunction into the eigenstate of the observable that corresponds to the observed eigenvalue. Another paradigm is protective measurements, which are able to preserve the coherence of the quantum state during the measurement process and allows the extraction of the expectation value of an observable by measuring a single quantum system [31].

A typical quantum control problem is formulated as the maximization of some objective functional (fidelity) that represents the desired property of the system to be optimized. An important topic is the analysis of the dynamic and kinematic quantum control landscapes [32–34]. The dynamical control landscape is defined as a graph of the objective functional as a functional of the control. The kinematic control landscape is formed by representing the dynamics of the controlled quantum system by transformation maps (e.g., by unitary transformations or Kraus maps) instead of differential evolution equations and considering the parameters of these maps as controls.

Key points of the control landscape are global maxima (for maximization of the objective) and global minima (for minimization of the objective). *Traps* are local but not global maxima (resp., minima) of the control landscape. An important type of critical point is the *second-order trap*—a critical point where the Hessian of the objective is negative (resp., positive) semi-definite but not strictly negative (resp., positive). At such points, the objective may still grow (resp., decrease) along directions in the control space that correspond to zero eigenvalues of the Hessian, but the growth is slower than the second order of small variations in the control. Second-order traps were introduced and studied in [33] (see also [35]). The importance of the analysis of kinematic control landscapes was shown for closed systems in [32]. For open quantum systems, the analysis of the kinematic control landscape was performed in [36], and a unified analysis for both quantum and classical systems was performed in [37]. Applications to problems in chemistry were found [38,39].

Quantum systems with dynamical symmetries are of particular interest in quantum control [6,8,40–42]. Such systems are not completely controllable by means of coherent control, while they may have no Hermitian observables that are invariant under *all* controls

(while for any particular control, such invariant observables may exist). Instead of that, they may have some different conservation laws. This symmetry can be broken using some kind of incoherent control, as was implemented, for example, using the back-action of non-selective quantum measurements in [6] for a three-level system with dynamical symmetry (see Figure 1). For this system, the maximum transition probability $P_{1 \rightarrow 2}$ between the ground and intermediate states using only coherent control was shown to be $1/2$ [41]. In [6], the maximum transition probability when coherent control was assisted by the non-selective measurement of the population of the ground state was computed and shown to be $0.004(\sqrt{393 - 48\sqrt{6}} + 138 + 7\sqrt{6}) \approx 0.687$. An important analysis of this system was performed in [8], where the following problem was considered and solved: find an observable such that its von Neumann measurement, along with coherent control, allows the initial state to be completely steered into a target state. In this case, the choice of the measured observable is considered as control according to [5].

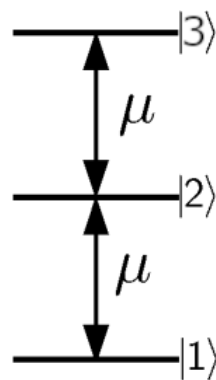


Figure 1. Energy level structure and allowed transitions between the energy levels of a three-level quantum system with dynamical symmetry. The maximum transition probability $|1\rangle \rightarrow |2\rangle$ using only coherent control is $1/2$.

In this work, we consider this three-level quantum system in more detail. We find and characterize all critical points of the transition probability $P_{1 \rightarrow 2}$, and in this sense, we completely describe its kinematic quantum control landscape, which we show consists of global maxima, global minima, saddle points and second-order traps. For comparison, we compute the maximum measurement-assisted transition probability $P_{1 \rightarrow 3}$ between the ground and upper excited states, as well as the maxima of both these transition probabilities when assisted by the measurement of the intermediate state $|2\rangle$.

The structure of this work is the following. Section 2 reviews the general idea of control using the back-action of quantum measurements. In Section 3, we provide the formulation of the considered problem. Section 4 contains necessary results from spin-1 representation theory. Section 5 contains preliminary computations of the measurement-assisted transition probabilities in the kinematic representation of controls. Section 6 contains a detailed analysis of the kinematic control landscape for the transition probability $P_{1 \rightarrow 2}$. Section 7 contains the computation of the maximum values of the transition probability $P_{1 \rightarrow 3}$ assisted by the measurement of state $|1\rangle$ or $|2\rangle$ and the transition probability $P_{1 \rightarrow 2}$ assisted by the measurement of state $|2\rangle$. The Discussion section (Section 8) summarizes the results.

2. Measurement-Assisted Quantum Control

In this section, we discuss in detail the scheme of quantum control using the back-action of non-selective quantum measurements in the formula introduced in [5].

Measurements performed on a quantum system are generally probabilistic: measurement outcomes for identical measurements performed on identically prepared quantum systems vary and are obtained with certain probabilities. Another important difference between quantum measurements and measurements performed on classical systems is that measurements of quantum systems not only allow the extraction of some

information about the system but also often change the state of the system, and such a state change can be significant.

Consider the non-selective measurement of a system observable $O = \sum_i \lambda_i P_i$ (a Hermitian operator) with eigenvalues $\lambda_i \in \mathbb{R}$ and spectral projectors P_i , $P_i = P_i^\dagger$, $P_i^2 = P_i$. Eigenvalues λ_i are the possible measurement outcomes. If ρ is the density matrix of the system before the measurement, then the measurement outcome λ_i is obtained with the probability $p_i = \text{Tr} \rho P_i$. If the observer looks at the measurement apparatus and reads the measurement outcome λ_i , then the system state immediately after the measurement will be transformed to $P_i \rho P_i / p_i$. This reduction is known as the collapse of the wavefunction. Non-selective measurement corresponds to a situation in which the «observer» does not look at the measurement apparatus and does not read the measurement outcome. The outcome for this situation can be described as the average of the realization of all possible measurement outcomes with their corresponding probabilities. In this situation, the measurement outcome is the average value $\langle O \rangle = \sum_i p_i \lambda_i = \text{Tr} \rho O$, and according to the von Neumann–Lüders postulate [43,44], the non-selective measurement of the observable O transforms the density matrix as follows:

$$\rho \rightarrow \mathcal{M}_O(\rho) = \sum_i P_i \rho P_i. \quad (1)$$

In particular, the non-selective measurement of a population $O = P_\psi = |\psi\rangle\langle\psi|$ of some state $|\psi\rangle$ transforms the density matrix as follows:

$$\rho \rightarrow \mathcal{M}_{P_\psi}(\rho) = P_\psi \rho P_\psi + (\mathbb{I} - P_\psi) \rho (\mathbb{I} - P_\psi), \quad (2)$$

where \mathbb{I} is the identity operator. In quantum control, quantum measurements can be used for real-time feedback, which was developed for models of quantum optics in [45–47]. In this scheme, some control (e.g., a shaped laser field) continuously acts on the controlled quantum system, and during this process, a discrete or continuous selective measurement of a certain observable is performed, and the measurement outcome is processed to modify the applied control in real time. Various achievements have been made in quantum feedback control. A coherent quantum feedback strategy was proposed [48]. The problem of quantum feedback control in the context of established formulations of classical control theory was discussed [49]. The Hamilton–Jacobi–Bellman equation for quantum optimal feedback control was derived [50]. The ability to simulate universal dynamical control through the repeated application of only two coherent control operations and a simple “Yes–No” measurement was shown [51]. To control the position and momentum of observables, the experimental measurement-based quantum control of the motion of a millimeter-sized membrane resonator was demonstrated [52]. An approach to information transfer in spintronics networks via the design of time-invariant feedback control laws without recourse to dynamic control was proposed [53]. Applications of quantum feedback to quantum engineering are discussed in the review in [54]. Measurement-based feedback cooling operating deep in the sideband-unresolved limit was demonstrated [55]. Feedback quantum control with deep reinforcement learning was applied to driving a system with double-well potential with high fidelity toward the ground state [56]. Feedback control was proposed for the control of a solid-state qubit [57], non-linear systems [58], quantum state manipulation [59], multi-qubit entanglement generation [60], the formation of coupled-qubit-based thermal machines [61], the steering of an energy function to the minimum energy eigenstate in variational quantum algorithms [29], etc.

Real-time feedback control can potentially be very powerful but is difficult to realize experimentally due to the need for fast real-time processing of the measurement outcome. However, since non-selective quantum measurements themselves modify the state of the system, they can potentially be used for control, even without feedback. Such a scheme has the advantage of not using fast real-time processing of the measurement outcome but at the cost of needing to measure various quantum observables. The mathematical formulation of using non-selective quantum measurements with or without coherent quantum control was developed in [5], where, apart from the general formulation, the two-level case was

completely analytically solved: in this case, the optimal measured observables and the maximum attained fidelity for maximizing the transition probability in a two-level quantum system by using any given number of non-selective measurements were analytically computed. The general formulation includes coherent or incoherent control during time intervals $[0, t_1), \dots, (t_k, t_{k+1}), \dots, (t_{N-1}, t_N]$, inducing the CPTP dynamical map $\Phi_{(t_k, t_{k+1})}$ in each interval and non-selective measurements of observables O_k at time moments t_k . The overall evolution of the initial density matrix ρ_0 will be

$$\rho(T) = \Phi_{(t_N, T)} \circ \mathcal{M}_{Q_N} \circ \Phi_{(t_{N-1}, t_N)} \circ \mathcal{M}_{Q_{N-1}} \circ \dots \circ \Phi_{(t_1, t_2)} \circ \mathcal{M}_{Q_1} \circ \Phi_{[0, t_1)}(\rho_0). \quad (3)$$

The control goal is to optimize, in addition to coherent and incoherent controls, the measured observables O_k to maximize a given control objective (e.g., to realize an optimal state transfer).

Another view on this type of quantum control can be described via the famous Zeno and anti-Zeno effects. The quantum Zeno effect, predicted by L. Khalfin [62,63] and B. Misra and E. C. G. Sudarshan [64], states that making continuous non-selective measurements of the population of some state of a quantum system, which has its own internal evolution, leads to the freezing of the system in the measured state, independent of the internal system evolution. It is reminiscent of the arrow paradox (aporia) of the Greek philosopher Zeno of Elea, where, for an observation of a flying arrow at any one (duration-less) instant of time, the arrow is neither moving to where it is, nor to where it is not. Then, it is concluded that, since at every instant of time, there is no motion occurring, if the arrow is motionless at every instant and if time is entirely composed of instants, then the motion of the arrow would be impossible. In the quantum anti-Zeno (or dynamical Zeno) effect [65], one performs a non-selective measurement of some time-dependent state $P_t = |\psi(t)\rangle\langle\psi(t)|$ of the quantum system, which evolves with its internal dynamics. As a result, in the limit of continuous measurements, independently of the internal dynamics, the system will follow the time-dependent state of the measured observable, so the system density matrix at time t will be $|\psi(t)\rangle\langle\psi(t)|$. The anti-Zeno effect can be used to control the quantum system if one considers the time-dependent measured observable to be the control. If $|\psi(T)\rangle = |\psi_{\text{target}}\rangle$, then the non-selective measurement of P_t via anti-Zeno dynamics transfers the system to the target state $|\psi_{\text{target}}\rangle$, thereby realizing the state transfer of the system. The complete realization of such a state transfer can be performed in the limit of the continuous measurement of the observable P_t , which can be difficult to perform. Therefore, a natural question is how to produce the best approximation of the anti-Zeno dynamics by using a fixed number N of quantum measurements. For the two-level case, such an optimal approximation of the anti-Zeno effect using N quantum measurements was found [5]. The maximum transition probability was computed to be

$$P_{i \rightarrow f}^{\max}(N) = \frac{1}{2} \left[1 + \left(\cos \frac{\Delta\varphi}{N+1} \right)^{N+1} \right] < 1,$$

where $\Delta\varphi$ is the angle between Bloch vectors of the initial and target states. The anti-Zeno effect is obtained in the limit of an infinite number of measurements when the interval between any two consecutive measurements tends to zero, $\lim_{N \rightarrow \infty} P_{i \rightarrow f}^{\max}(N) = 1$.

Thus, in this work, the scheme of control using the back-action of non-selective measurements based on [5] is different from both quantum feedback control and Zeno-type control. It is different from feedback since it does not read the measurement outcome. It is different from Zeno-type control since it uses a finite number of measurements. These differences lead to advantages and disadvantages. The advantages include the simpler experimental realization, since there is no need for real-time feedback and no need for continuous measurements. The potential disadvantage is the lower efficiency of control. How significant this decrease in efficiency is, of course, depends on the particular control problem and the sufficient level of fidelity that one needs to obtain.

3. Formulation of the Problem

We consider a three-level quantum system with dynamical symmetry, with the free and interaction Hamiltonians defined as (we set the Planck constant $\hbar = 1$)

$$H_0 = \begin{pmatrix} 0 & 0 & 0 \\ 0 & 1 & 0 \\ 0 & 0 & 2 \end{pmatrix}, \quad V = \mu \begin{pmatrix} 0 & 1 & 0 \\ 1 & 0 & 1 \\ 0 & 1 & 0 \end{pmatrix}. \quad (4)$$

The energy level structure of this system is shown in Figure 1. Without loss of generality, one can set $\mu = 1$. Physically, such a Hamiltonian represents a three-level system whose interaction with the laser field consists of a dipolar interaction, with constant dipolar terms coupling only neighboring states, and is equivalent to a spin-1 particle, which was studied in [40]. The coherent dynamics of more general spin-like quantum systems was studied in [66]. The controllability of such a system was studied in [41], where it was shown that, such a system is not completely controllable by only coherent control. As mentioned above, the maximum transition probability for coherent control assisted by a single von Neumann measurement of the population of the ground state for this system is $0.004(\sqrt{393 - 48\sqrt{6}} + 138 + 7\sqrt{6}) \approx 0.687$ [6]. In [8], the problem of finding an observable such that its von Neumann measurement along with coherent control allows the complete steering of the initial state into a target state was solved.

The unitary evolution operator of this system evolving under the action of a coherent control $f \in L^2([0, T]; \mathbb{R})$ satisfies the Schrödinger equation:

$$\frac{dU_t^f}{dt} = -i(H_0 + f(t)V)U_t^f, \quad U_{t=0}^f = \mathbb{I}. \quad (5)$$

where \mathbb{I} is a 3×3 identity matrix. The time-evolved pure state of this system can be written as

$$|\psi(t)\rangle = U_t^f |\psi(0)\rangle = C_1(t)|1\rangle + C_2(t)|2\rangle + C_3(t)|3\rangle, \quad C_i(t) \in \mathbb{C}, \quad i = 1, 2, 3$$

The coefficients in this expansion satisfy the normalization condition $|C_1(t)|^2 + |C_2(t)|^2 + |C_3(t)|^2 = 1$.

While this system is not controllable, it has no Hermitian observable that is conserved by *all* controls, i.e., there is no Hermitian observable O such that for any f , $[H_0 + f(t)V, O] = 0$ (if such an observable existed, its average value would be determined by the initial state and could not be modified by any control). Indeed, this condition can be satisfied for any f only if $[H_0, O] = [V, O] = 0$, which holds only for $O = \text{const} \cdot \mathbb{I}$, as can be directly checked. For any particular control f , an invariant operator exists, as was shown in [67], where such an operator was even explicitly constructed; however, this invariant operator depends on f . Instead of the absence of an f -independent conserved Hermitian operator, it is known [41] that this system has the conservation law

$$\left| C_1(t)C_2(t) - \frac{C_3(t)^2}{2} \right| = \text{Const}. \quad (6)$$

Note that the quantity under the modulus in this constraint is also conserved. This conservation law, as was shown in [41], limits the maximum transition probability $P_{1 \rightarrow 2}(f)$ from state $|1\rangle$ to state $|2\rangle$ over all coherent controls f to

$$\max_f P_{1 \rightarrow 2}(f) = \frac{1}{2}.$$

The transition probability is computed as $P_{1 \rightarrow 2}(f) = |C_2(T)|^2$ for a large enough T , where the coefficients satisfy the initial condition $C_1(0) = 1, C_2(0) = C_3(0) = 0$.

Consider now the non-selective measurement of a system observable O (a Hermitian operator) with spectral projectors P_i . If ρ is the density matrix of the system before the

measurement, then the non-selective measurement of O transforms the density according to Equation (1). In particular, the non-selective measurement of a population $O = P_\psi = |\psi\rangle\langle\psi|$ of some state $|\psi\rangle$ transforms the density matrix according to Equation (2).

Suppose that the quantum system (4) evolves under the action of a coherent control f_1 during the time interval $[-T_1, 0)$ with some sufficiently long time $T_1 \geq T^*$; then, at $t = 0$, the non-selective measurement of the population of some state $|\psi\rangle$ is performed, and finally, during the time interval $(0, T_2]$ with $T_2 \geq T^*$, the system again evolves under the action of some coherent control f_2 . Here, T^* is the minimal time during which all allowed unitary evolutions can be generated. Then, its final density matrix at $t = T_2$ will be

$$\rho(T_2) = U_{f_2} \mathcal{M}_{P_\psi} [U_{f_1} \rho(-T_1) U_{f_1}^\dagger] U_{f_2}^\dagger. \tag{7}$$

In particular, the probabilities of transitions from state $|1\rangle$ to state $|2\rangle$ and from state $|1\rangle$ to state $|3\rangle$ when the measurement of the population of either $|\psi\rangle = |1\rangle$ or $|\psi\rangle = |2\rangle$ is performed are defined by setting $\rho(-T_1) = |1\rangle\langle 1|$ in (7):

$$P_{1 \rightarrow k}(f_1, \mathcal{M}_{|j\rangle\langle j|}, f_2) = \langle k | U_{f_2} \mathcal{M}_{|j\rangle\langle j|} (U_{f_1} |1\rangle\langle 1| U_{f_1}^\dagger) U_{f_2}^\dagger |k\rangle, \tag{8}$$

where $k = 2, 3$ and $j = 1, 2$. Numerically constructed kinematic control landscapes are plotted in Figure 2. Below, we perform a theoretical analysis of these control landscapes.

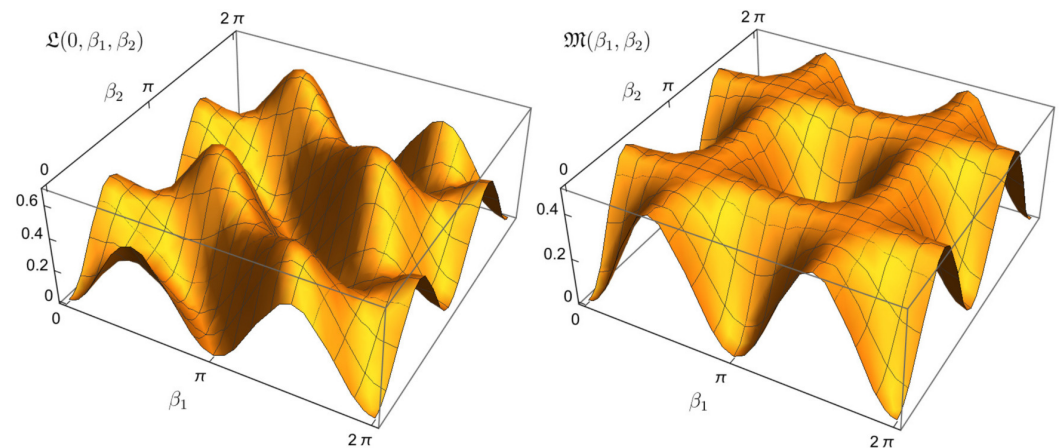


Figure 2. Kinematic control landscapes of the transition probability $P_{1 \rightarrow 2}(U(1), \mathcal{M}_{|i\rangle\langle i|}, U(2))$. **(Left):** $i = 1$ and $\Omega = 0$ (i.e., plot of the function $\mathfrak{L}(0, \beta_1, \beta_2)$; see below). **(Right):** $i = 2$ (i.e., plot of the function $\mathfrak{M}(\beta_1, \beta_2)$; see below). The left landscape has second-order traps (see Theorem 1), whereas the right landscape is completely trap-free (see Theorem 3).

4. Spin-1 Representation Theory

Since we are studying the kinematic control landscape of a system under two coherent controls, we need to consider the manifold

$$\mathcal{R} \times \mathcal{R}, \quad \mathcal{R} = \{U \in SU(3) \mid U \in \text{spin-1 representation of } SU(2) \text{ Lie group}\}. \tag{9}$$

Now, we describe the parameterization of \mathcal{R} .

For this system, the free and interaction Hamiltonians generate a spin-1 representation of the Lie algebra $\mathfrak{su}(2)$. Let J_x, J_y and J_z be standard generators of the spin-1 representation of the Lie algebra $\mathfrak{su}(2)$ with matrices

$$J_x = \frac{1}{\sqrt{2}} \begin{pmatrix} 0 & 1 & 0 \\ 1 & 0 & 1 \\ 0 & 1 & 0 \end{pmatrix}, \quad J_y = \frac{1}{\sqrt{2}} \begin{pmatrix} 0 & -i & 0 \\ i & 0 & -i \\ 0 & i & 0 \end{pmatrix}, \quad J_z = \begin{pmatrix} 1 & 0 & 0 \\ 0 & 0 & 0 \\ 0 & 0 & -1 \end{pmatrix},$$

which are written in the eigenbasis of J_z denoted by $\{|1, -1\rangle, |1, 0\rangle, |1, 1\rangle\}$, where the first value denotes spin, and the second value denotes spin projection. Below, we use the notation $|1, -1\rangle \equiv |1\rangle, |1, 0\rangle \equiv |2\rangle, |1, 1\rangle \equiv |3\rangle$.

In the kinematic representation, we consider the allowed evolution operators given by Wigner’s D-matrices, which are parameterized by Euler angles α, β, γ [68,69].

The first parameterization that we use is

$$U(\alpha, \beta, \gamma) = e^{-i\alpha J_z} \cdot e^{-i\beta J_y} \cdot e^{-i\gamma J_z},$$

which we call ZYZ parameterization. It is defined for $(\alpha, \beta, \gamma) \in (-\pi, \pi] \times [0, \pi) \times (-\pi, \pi]$. For $\beta = 0$, one has

$$U(\alpha, 0, \gamma) = \begin{pmatrix} e^{-i(\alpha+\gamma)} & 0 & 0 \\ 0 & 1 & 0 \\ 0 & 0 & e^{i(\alpha+\gamma)} \end{pmatrix},$$

so different pairs of α and γ with the same $\alpha + \gamma$ determine one unitary operator [70]. The subset

$$\mathcal{B} := \{U \in \mathcal{R} \mid U = \text{diag}(e^{-i\phi}, 1, e^{i\phi}), \phi \in [0, 2\pi)\} \subset \mathcal{R} \tag{10}$$

has to be parameterized in another way.

The second parameterization is

$$U(\alpha, \beta, \gamma) = e^{-i\alpha J_y} \cdot e^{-i\beta J_z} \cdot e^{-i\gamma J_y},$$

which we call YZY parameterization. It is determined for $(\alpha, \beta, \gamma) \in (-\pi, \pi] \times [0, \pi) \times (-\pi, \pi]$ and has the same degeneracy for $\beta = 0$.

The two matrix exponents appearing in both parameterizations have the form

$$e^{-i\phi J_y} = \frac{1}{2} \begin{pmatrix} 1 + \cos \phi & -\sqrt{2} \sin \phi & 1 - \cos \phi \\ \sqrt{2} \sin \phi & \cos \phi & -\sqrt{2} \sin \phi \\ 1 - \cos \phi & \sqrt{2} \sin \phi & 1 + \cos \phi \end{pmatrix}, \tag{11}$$

$$e^{-i\phi J_z} = \begin{pmatrix} e^{-i\phi} & 0 & 0 \\ 0 & 1 & 0 \\ 0 & 0 & e^{i\phi} \end{pmatrix}. \tag{12}$$

5. Transition Probabilities Driven by Coherent Control Assisted by One Non-Selective Measurement

Coherent controls f_1 and f_2 are called *dynamic controls*. The dynamic control landscape is defined as a graph of the transition probability $P_{1 \rightarrow 2}(f_1, f_2)$, considered as a functional of coherent controls f_1 and f_2 . For the control landscape analysis, it is convenient to consider coherent controls as elements of the L^2 space so that the transition probability becomes a functional $P_{1 \rightarrow 2} : L^2 \times L^2 \rightarrow [0, 1]$ (not necessarily a surjection).

Kinematic controls are parameters determining allowed unitary evolutions, which are elements of \mathcal{R} . Below, we consider the transition probabilities as functions of the kinematic controls, as in [6]. In the kinematic representation, the system during the first period of evolution evolves with some unitary evolution operator $U(1) = U^{f_1}$, defined by Equation (5) with $f = f_1$, and then one performs a non-selective measurement (we consider the measurement of the population of either state $|1\rangle$ or $|2\rangle$), and finally, after the measurement, the system evolves with another evolution operator $U(2) = U^{f_2}$, defined by Equation (5) with $f = f_2$.

The transition probabilities in the kinematic representation, i.e., as functions on $\mathcal{R} \times \mathcal{R}$, become

$$P_{1 \rightarrow k}(U(1), \mathcal{M}_{|j\rangle\langle j|}, U(2)) = \langle k | U(2) \mathcal{M}_{|j\rangle\langle j|} [U(1) |1\rangle \langle 1| U^\dagger(1)] U^\dagger(2) |k\rangle. \tag{13}$$

Below, we consider $k = 2, 3$ and $j = 1, 2$. We mainly concentrate on the most non-trivial case, i.e., $k = 2, j = 1$, for which we study the kinematic landscape in detail. For comparison,

in Section 7, we also compute the maximum transition probabilities for the cases $(k, j) = (2, 2), (3, 1), (3, 2)$ and numerically plot some of the corresponding control landscapes.

The initial system state (before the application of coherent control f_1) is $\rho(-T_1) = |1\rangle\langle 1|$. The first control transforms the initial state into

$$\rho(0-) = U(1)|1\rangle\langle 1|U^\dagger(1).$$

Consider the case $j = 1$. After performing the non-selective measurement of $P_{|1\rangle} = |1\rangle\langle 1|$, the system density matrix will be

$$\begin{aligned} \rho(0+) &= P_{|1\rangle}\rho(0-)P_{|1\rangle} + (\mathbb{I} - P_{|1\rangle})\rho(0-)(\mathbb{I} - P_{|1\rangle}) = |U_{11}(1)|^2|1\rangle\langle 1| \\ &+ |U_{21}(1)|^2|2\rangle\langle 2| + |U_{31}(1)|^2|3\rangle\langle 3| + U_{21}(1)\overline{U_{31}(1)}|2\rangle\langle 3| + \overline{U_{21}(1)}U_{31}(1)|3\rangle\langle 2|. \end{aligned}$$

Finally,

$$\begin{aligned} \langle k|\rho(T_2)|k\rangle &= \langle k|U(2)\rho(0+)U^\dagger(2)|k\rangle = |U_{11}(1)|^2|U_{k1}(2)|^2 + |U_{21}(1)|^2|U_{k2}(2)|^2 \\ &+ |U_{31}(1)|^2|U_{k3}(2)|^2 + 2\text{Re}[U_{21}(1)\overline{U_{31}(1)}U_{k2}(2)\overline{U_{k3}(2)}]. \end{aligned} \tag{14}$$

Consider the case $j = 2$. After performing the non-selective measurement of $P_{|2\rangle} = |2\rangle\langle 2|$, the system density matrix will be

$$\begin{aligned} \rho(0+) &= P_{|2\rangle}\rho(0-)P_{|2\rangle} + (\mathbb{I} - P_{|2\rangle})\rho(0-)(\mathbb{I} - P_{|2\rangle}) = |U_{11}(1)|^2|1\rangle\langle 1| \\ &+ |U_{21}(1)|^2|2\rangle\langle 2| + |U_{31}(1)|^2|3\rangle\langle 3| + U_{11}(1)\overline{U_{31}(1)}|1\rangle\langle 3| + \overline{U_{11}(1)}U_{31}(1)|3\rangle\langle 1|. \end{aligned}$$

Finally,

$$\begin{aligned} \langle k|\rho(T_2)|k\rangle &= \langle k|U(2)\rho(0+)U^\dagger(2)|k\rangle = |U_{11}(1)|^2|U_{k1}(2)|^2 + |U_{21}(1)|^2|U_{k2}(2)|^2 \\ &+ |U_{31}(1)|^2|U_{k3}(2)|^2 + 2\text{Re}[U_{11}(1)\overline{U_{31}(1)}U_{k2}(2)\overline{U_{k3}(2)}]. \end{aligned} \tag{15}$$

6. Kinematic Quantum Control Landscape of the Transition Probability

The kinematic control landscape is a function on $\mathcal{R} \times \mathcal{R}$, and from Equation (14), we know that the kinematic landscape of the transition probability is

$$\begin{aligned} P_{1 \rightarrow 2}(U(1), \mathcal{M}_{|1\rangle\langle 1|}, U(2)) &= |U_{11}(1)|^2|U_{21}(2)|^2 + |U_{21}(1)|^2|U_{22}(2)|^2 + |U_{31}(1)|^2|U_{23}(2)|^2 \\ &+ 2\text{Re}[U_{21}(1)\overline{U_{31}(1)}U_{22}(2)\overline{U_{23}(2)}]. \end{aligned} \tag{16}$$

Since we consider the three-dimensional representation of the $SU(2)$ Lie group, we choose Euler angle parameterization (see Section 4) to study the kinematic control landscape. The parameters (α, β, γ) in the unitary evolution operator (17) are called *kinematic controls*. We denote $c_i = (\alpha_i, \beta_i, \gamma_i)$ for $i = 1, 2$. Thus, the transition probability is considered as a function of the kinematic control parameters $(\alpha_1, \beta_1, \gamma_1, \alpha_2, \beta_2, \gamma_2)$ on the corresponding open charts.

First, we consider ZYZ parameterization to find critical points on $(\mathcal{R} \setminus \mathcal{B}) \times (\mathcal{R} \setminus \mathcal{B})$. From (11) and (12), we obtain the following matrix representation of the evolution operator:

$$U(\alpha, \beta, \gamma) = \begin{pmatrix} e^{-i(\alpha+\gamma)} \cos^2 \frac{\beta}{2} & -\frac{e^{-i\alpha}}{\sqrt{2}} \sin \beta & e^{-i(\alpha-\gamma)} \sin^2 \frac{\beta}{2} \\ \frac{e^{-i\gamma}}{\sqrt{2}} \sin \beta & \cos \beta & -\frac{e^{i\gamma}}{\sqrt{2}} \sin \beta \\ e^{i(\alpha-\gamma)} \sin^2 \frac{\beta}{2} & \frac{e^{i\alpha}}{\sqrt{2}} \sin \beta & e^{i(\alpha+\gamma)} \cos^2 \frac{\beta}{2} \end{pmatrix}. \tag{17}$$

Using (17), we obtain

$$P_{1 \rightarrow 2}(c_1, \mathcal{M}_{|1\rangle\langle 1|}, c_2) =$$

$$= \frac{1}{8} \sin^2 \beta_2 (3 + \cos 2\beta_1) + \frac{1}{2} \sin^2 \beta_1 \cos^2 \beta_2 - \frac{1}{2} \cos \Omega \sin \beta_1 \sin^2 \frac{\beta_1}{2} \sin 2\beta_2 =: \mathcal{L}_1(\Omega, \beta_1, \beta_2),$$

where $\Omega = \alpha_1 + \gamma_2$, and \mathcal{L}_1 is the control landscape function. Hence, the transition probability $P_{1 \rightarrow 2}(c_1, \mathcal{M}_{|1\rangle\langle 1|}, c_2)$ is a function of only three kinematic parameters: Ω, β_1 and β_2 .

The domain of the graph is $(\Omega, \beta_1, \beta_2) \in (-\pi, \pi] \times (0, \pi) \times (0, \pi)$. For $\Omega = 0$, the kinematic landscape of the transition probability $P_{1 \rightarrow 2}(c_1, \mathcal{M}_{|1\rangle\langle 1|}, c_2) = \mathcal{L}_1(0, \beta_1, \beta_2)$ is shown in Figure 2. As mentioned in the Introduction, in [6], it was shown that

$$\max_{c_1, c_2} P_{1 \rightarrow 2}(c_1, \mathcal{M}_{|1\rangle\langle 1|}, c_2) = 0.004 \times (\sqrt{393 - 48\sqrt{6}} + 138 + 7\sqrt{6}). \tag{18}$$

Lemma 1. All critical points of $\mathcal{L}_1(\Omega, \beta_1, \beta_2)$, their types and the corresponding values of the function are given in Table 1.

Table 1. Critical points, their types and values of the objective function $\mathcal{L}_1(\Omega, \beta_1, \beta_2)$.

$(\Omega, \beta_1, \beta_2)$	$P_{1 \rightarrow 2}$	Type of Point
$(\pm \frac{\pi}{2}, \frac{\pi}{2}, \frac{\pi}{2})$	1/4	Saddle point
$(\pi, \arccos(\frac{-1+\sqrt{5}}{2}), \pi - \frac{1}{2} \arctan(2\sqrt{2 + \sqrt{5}}))$, $(0, \arccos(\frac{-1+\sqrt{5}}{2}), \frac{1}{2} \arctan(2\sqrt{2 + \sqrt{5}}))$	1/4	Saddle point
$(\pi, \arccos(\frac{1+\sqrt{6}}{5}), \frac{1}{2} \arccos(\frac{1}{1-\sqrt{6}}))$, $(0, \arccos(\frac{1+\sqrt{6}}{5}), \pi - \frac{1}{2} \arccos(\frac{1}{1-\sqrt{6}}))$	$\frac{3}{50}(9 - \sqrt{6}) \approx 0.393$	Saddle point
$(\pi, \arccos(\frac{1-\sqrt{6}}{5}), \frac{1}{2} \arccos(\frac{1}{1+\sqrt{6}}))$, $(0, \arccos(\frac{1-\sqrt{6}}{5}), \pi - \frac{1}{2} \arccos(\frac{1}{1+\sqrt{6}}))$	$\frac{3}{50}(9 + \sqrt{6}) \approx 0.687$	Global maximum

Proof. Let us find critical points of the function $\mathcal{L}_1(\Omega, \beta_1, \beta_2)$ on the domain $(-\pi, \pi] \times (0, \pi) \times (0, \pi)$. The derivatives of $\mathcal{L}_1(\Omega, \beta_1, \beta_2)$ are:

$$\begin{cases} \mathcal{L}_1(\Omega, \beta_1, \beta_2)'_{\Omega} = \frac{1}{2} \sin \Omega \sin \beta_1 \sin^2 \frac{\beta_1}{2} \sin 2\beta_2 \\ \mathcal{L}_1(\Omega, \beta_1, \beta_2)'_{\beta_1} = \frac{1}{8}(1 + 3 \cos 2\beta_2) \sin 2\beta_1 - \frac{1}{4} \cos \Omega (\cos \beta_1 - \cos 2\beta_1) \sin 2\beta_2 \\ \mathcal{L}_1(\Omega, \beta_1, \beta_2)'_{\beta_2} = \frac{1}{8}(1 + 3 \cos 2\beta_1) \sin 2\beta_2 - \frac{1}{2} \cos \Omega \sin \beta_1 \cos 2\beta_2 (1 - \cos \beta_1) \end{cases} .$$

For later analysis, we will need the Hessian of $\mathcal{L}_1(\Omega, \beta_1, \beta_2)$:

$$\begin{cases} \mathcal{L}_1(\Omega, \beta_1, \beta_2)''_{\Omega\Omega} = \frac{1}{2} \cos \Omega \sin^2 \frac{\beta_1}{2} \sin \beta_1 \sin 2\beta_2 \\ \mathcal{L}_1(\Omega, \beta_1, \beta_2)''_{\Omega\beta_1} = \sin \Omega \sin^2 \frac{\beta_1}{2} \sin \beta_2 (2 \cos \beta_1 + 1) \cos \beta_2 \\ \mathcal{L}_1(\Omega, \beta_1, \beta_2)''_{\Omega\beta_2} = \sin \Omega \sin^2 \frac{\beta_1}{2} \sin \beta_1 \cos 2\beta_2 \\ \mathcal{L}_1(\Omega, \beta_1, \beta_2)''_{\beta_1\beta_1} = \frac{1}{4} \cos \Omega (\sin \beta_1 - 2 \sin 2\beta_1) \sin 2\beta_2 + \cos 2\beta_1 (3 \cos 2\beta_2 + 1) \\ \mathcal{L}_1(\Omega, \beta_1, \beta_2)''_{\beta_1\beta_2} = -\cos \Omega \sin^2 \frac{\beta_1}{2} (2 \cos \beta_1 + 1) \cos 2\beta_2 - \frac{3}{4} \sin 2\beta_1 \sin 2\beta_2 \\ \mathcal{L}_1(\Omega, \beta_1, \beta_2)''_{\beta_2\beta_2} = 2 \cos \Omega \sin \beta_1 \sin 2\beta_2 \sin^2 \frac{\beta_1}{2} + \frac{1}{4} (3 \cos 2\beta_1 + 1) \cos 2\beta_2 \end{cases} .$$

We search for all the points where the gradient of \mathcal{L}_1 is zero, i.e., $\nabla \mathcal{L}_1(\Omega, \beta_1, \beta_2) = 0$. From the condition $\mathcal{L}_1(\Omega, \beta_1, \beta_2)'_{\Omega} = 0$, we determine that such extreme points should lie on the surfaces:

$$\begin{cases} \Omega = 0, \pi \\ \beta_2 = \frac{\pi}{2} \end{cases} .$$

Consider these cases separately.

1. $\beta_2 = \frac{\pi}{2}$. In this case ,

$$\begin{cases} \mathcal{L}_1(\Omega, \beta_1, \frac{\pi}{2})'_{\beta_1} = -\frac{1}{4} \sin 2\beta_1 \\ \mathcal{L}_1(\Omega, \beta_1, \frac{\pi}{2})'_{\beta_2} = \cos \Omega \sin \beta_1 \sin^2 \frac{\beta_1}{2} \end{cases} .$$

Thus, from the conditions $\mathcal{L}_1(\Omega, \beta_1, \frac{\pi}{2})'_{\beta_1} = \mathcal{L}_1(\Omega, \beta_1, \frac{\pi}{2})'_{\beta_2} = 0$, we find the critical points $(\pm \frac{\pi}{2}, \frac{\pi}{2}, \frac{\pi}{2})$. The Hessian has the form

$$H_{\mathcal{L}_1}\left(-\frac{\pi}{2}, \frac{\pi}{2}, \frac{\pi}{2}\right) = \begin{pmatrix} 0 & 0 & \frac{1}{2} \\ 0 & \frac{1}{2} & 0 \\ \frac{1}{2} & 0 & \frac{1}{2} \end{pmatrix},$$

$$H_{\mathcal{L}_1}\left(\frac{\pi}{2}, \frac{\pi}{2}, \frac{\pi}{2}\right) = \begin{pmatrix} 0 & 0 & -\frac{1}{2} \\ 0 & \frac{1}{2} & 0 \\ -\frac{1}{2} & 0 & \frac{1}{2} \end{pmatrix}.$$

One has $\mathcal{L}_1(\pm \frac{\pi}{2}, \frac{\pi}{2}, \frac{\pi}{2}) = \frac{1}{4}$. Computing Hessian eigenvalues allows us to conclude that these are saddle points.

2. $\Omega = \pi$.
In this case,

$$\begin{cases} \mathcal{L}_1(\pi, \beta_1, \beta_2)'_{\beta_1} = \frac{1}{8}(1 + 3 \cos 2\beta_2) \sin 2\beta_1 + \frac{1}{4}(\cos \beta_1 - \cos 2\beta_1) \sin 2\beta_2 = 0 \\ \mathcal{L}_1(\pi, \beta_1, \beta_2)'_{\beta_2} = \frac{1}{8}(1 + 3 \cos 2\beta_1) \sin 2\beta_2 + \frac{1}{2} \sin \beta_1 \cos 2\beta_2(1 - \cos \beta_1) = 0 \end{cases} . \tag{19}$$

which is equivalent to

$$\begin{cases} (1 + 3 \cos 2\beta_2) \sin 2\beta_1 = 2(\cos 2\beta_1 - \cos \beta_1) \sin 2\beta_2 \\ 4 \sin \beta_1 \cos 2\beta_2(\cos \beta_1 - 1) = (1 + 3 \cos 2\beta_1) \sin 2\beta_2 \end{cases} .$$

Dividing the second equation by the first, we obtain

$$\frac{\cos \beta_1(1 + 3 \cos 2\beta_2)}{2 \cos 2\beta_2(\cos \beta_1 - 1)} = \frac{2(\cos 2\beta_1 - \cos \beta_1)}{1 + 3 \cos 2\beta_1},$$

from which we can express $1/\cos 2\beta_2$ in terms of $\cos \beta_1 \equiv x$ as

$$\frac{1}{\cos 2\beta_2} = \frac{4(\cos 2\beta_1 - \cos \beta_1)(\cos \beta_1 - 1)}{\cos \beta_1(1 + 3 \cos 2\beta_1)} - 3 = \frac{2(2x^2 - 1 - x)(x - 1)}{x(3x^2 - 1)} - 3.$$

We notice that $\cos \beta_1 = 1$ (which means that $\beta_1 = 0$) satisfies (19) for $\beta_2 = \frac{\pi}{2}$. Let us express $\tan 2\beta_2$ from the second equation in (19):

$$\tan 2\beta_2 = 4 \sin \beta_1 \frac{\cos \beta_1 - 1}{1 + 3 \cos 2\beta_1} = 2\sqrt{1 - x^2} \frac{x - 1}{3x^2 - 1}.$$

Using the trigonometric identity

$$\frac{1}{\cos^2 2\beta_2} = 1 + \tan^2 2\beta_2,$$

we obtain the following equation for x :

$$\left(\frac{2(2x^2 - 1 - x)(x - 1)}{x(3x^2 - 1)} - 3\right)^2 = 1 + 4 \frac{(x - 1)^2(1 - x^2)}{(3x^2 - 1)^2}. \tag{20}$$

(We also need to consider $\cos 2\beta_1 = -\frac{1}{3}$ and $\cos \beta_1 = 0$ to make sure that we have not lost any solutions. From the system in (19), we notice that these two cases are not solutions for any β_2).

Equation (20) can be solved analytically. Finally, we have

$$(x + 1)^2 \left(x - \frac{-1 - \sqrt{5}}{2}\right) \left(x - \frac{-1 + \sqrt{5}}{2}\right) \left(x - \frac{1 - \sqrt{6}}{5}\right) \left(x - \frac{1 + \sqrt{6}}{5}\right) = 0.$$

Finding (β_1, β_2) from this equation, combined with the results obtained previously, we obtain the following critical points (which could be either extrema or saddle points):

$$\left[\begin{array}{l} (\beta_1^I, \beta_2^I) = \left(\arccos\left(\frac{1+\sqrt{6}}{5}\right), \frac{1}{2} \arccos\left(\frac{1}{1-\sqrt{6}}\right)\right) \approx (0.810, 1.166) \\ (\beta_1^{II}, \beta_2^{II}) = \left(\arccos\left(\frac{1-\sqrt{6}}{5}\right), \frac{1}{2} \arccos\left(\frac{1}{1+\sqrt{6}}\right)\right) \approx (1.865, 0.638) \\ (\beta_1^{III}, \beta_2^{III}) = \left(\arccos\left(\frac{-1+\sqrt{5}}{2}\right), \pi - \frac{1}{2} \arctan\left(2\sqrt{2 + \sqrt{5}}\right)\right) \approx (0.905, 2.475) \end{array} \right. \quad (21)$$

The corresponding values of the objective function are

$$\mathfrak{L}_1(\Omega, \beta_1, \beta_2) = \left[\begin{array}{l} \frac{1}{4}, \quad (\pi, \beta_1^{III}, \beta_2^{III}) \\ \frac{3}{50}(9 - \sqrt{6}), \quad (\pi, \beta_1^I, \beta_2^I) \\ \frac{3}{50}(9 + \sqrt{6}), \quad (\pi, \beta_1^{II}, \beta_2^{II}) \end{array} \right].$$

We compute the second derivatives to determine the type of each of these critical points:

$$\left\{ \begin{array}{l} \mathfrak{L}_1(\pi, \beta_1, \beta_2)''_{\Omega\Omega} = -\frac{1}{2} \sin^2 \frac{\beta_1}{2} \sin \beta_1 \sin 2\beta_2 \\ \mathfrak{L}_1(\pi, \beta_1, \beta_2)''_{\beta_1\beta_1} = \frac{1}{4} [(2 \sin 2\beta_1 - \sin \beta_1) \sin 2\beta_2 + \cos 2\beta_1 (3 \cos 2\beta_2 + 1)] \\ \mathfrak{L}_1(\pi, \beta_1, \beta_2)''_{\beta_1\beta_2} = \sin^2 \frac{\beta_1}{2} (2 \cos \beta_1 + 1) \cos 2\beta_2 - \frac{3}{4} \sin 2\beta_1 \sin 2\beta_2 \\ \mathfrak{L}_1(\pi, \beta_2, \beta_2)''_{\beta_2\beta_2} = \frac{1}{4} (3 \cos 2\beta_1 + 1) \cos 2\beta_2 - 2 \sin^2 \frac{\beta_1}{2} \sin \beta_1 \sin 2\beta_2 \end{array} \right.$$

(Only non-zero derivatives are written.) The Hessian matrix at the corresponding points is

$$\begin{aligned} H_{\mathfrak{L}_1}(\pi, \beta_1^I, \beta_2^I) &= \begin{pmatrix} \frac{1}{250}(13\sqrt{6} - 42) & 0 & 0 \\ 0 & \frac{1}{100}(23\sqrt{6} - 32) & \frac{1}{50}(-8 - 13\sqrt{6}) \\ 0 & \frac{1}{50}(-8 - 13\sqrt{6}) & \frac{1}{5}(\sqrt{6} - 4) \end{pmatrix} \\ H_{\mathfrak{L}_1}(\pi, \beta_1^{II}, \beta_2^{II}) &= \begin{pmatrix} \frac{1}{250}(-42 - 13\sqrt{6}) & 0 & 0 \\ 0 & \frac{1}{100}(-32 - 23\sqrt{6}) & \frac{1}{50}(13\sqrt{6} - 8) \\ 0 & \frac{1}{50}(13\sqrt{6} - 8) & \frac{1}{5}(-4 - \sqrt{6}) \end{pmatrix} \\ H_{\mathfrak{L}_1}(\pi, \beta_1^{III}, \beta_2^{III}) &= \begin{pmatrix} \frac{1}{4}(7 - 3\sqrt{5}) & 0 & 0 \\ 0 & \frac{1}{2}(\sqrt{5} - 3) & \frac{1}{4}(1 + \sqrt{5}) \\ 0 & \frac{1}{4}(1 + \sqrt{5}) & \frac{1}{4}(\sqrt{5} - 1) \end{pmatrix} \end{aligned}$$

From Sylvester’s criterion, we conclude that

$$\left[\begin{array}{l} \mathfrak{L}_1(\pi, \beta_1^{III}, \beta_2^{III}) = \frac{1}{4} - \text{saddle point} \\ \mathfrak{L}_1(\pi, \beta_1^I, \beta_2^I) = \frac{3}{50}(9 - \sqrt{6}) \approx 0.393 - \text{saddle point} \\ \mathfrak{L}_1(\pi, \beta_1^{II}, \beta_2^{II}) = \frac{3}{50}(9 + \sqrt{6}) \approx 0.687 - \text{global maximum} \end{array} \right.$$

3. $\Omega = 0$.

All the critical points are easily found from (21):

$$\begin{cases} (\beta_1^I, \beta_2^I) = \left(\arccos\left(\frac{1+\sqrt{6}}{5}\right), \pi - \frac{1}{2} \arccos\left(\frac{1}{1-\sqrt{6}}\right) \right) \approx (0.810, 1.975) \\ (\beta_1^{II}, \beta_2^{II}) = \left(\arccos\left(\frac{1-\sqrt{6}}{5}\right), \pi - \frac{1}{2} \arccos\left(\frac{1}{1+\sqrt{6}}\right) \right) \approx (1.865, 2.503) \\ (\beta_1^{III}, \beta_2^{III}) = \left(\arccos\left(\frac{-1+\sqrt{5}}{2}\right), \frac{1}{2} \arctan\left(2\sqrt{2+\sqrt{5}}\right) \right) \approx (0.905, 2.475) \end{cases} \quad (22)$$

In the same way as for the case $\Omega = \pi$, we compute the second derivative to determine type of each of the critical points:

$$\begin{cases} \mathcal{L}_1(0, \beta_1, \beta_2)''_{\Omega\Omega} = \frac{1}{2} \sin^2 \frac{\beta_1}{2} \sin \beta_1 \sin 2\beta_2 \\ \mathcal{L}_1(0, \beta_1, \beta_2)''_{\beta_1\beta_1} = \frac{1}{4} [(\sin \beta_1 - 2 \sin 2\beta_1) \sin 2\beta_2 + \cos 2\beta_1 (3 \cos 2\beta_2 + 1)] \\ \mathcal{L}_1(0, \beta_1, \beta_2)''_{\beta_1\beta_2} = -\frac{3}{4} \sin 2\beta_1 \sin 2\beta_2 - \sin^2 \frac{\beta_1}{2} (2 \cos \beta_1 + 1) \cos 2\beta_2 \\ \mathcal{L}_1(0, \beta_2, \beta_2)''_{\beta_2\beta_2} = 2 \sin \beta_1 \sin 2\beta_2 \sin^2 \frac{\beta_1}{2} + \frac{1}{4} (3 \cos 2\beta_1 + 1) \cos 2\beta_2 \end{cases}$$

The Hessian matrix at the corresponding points is

$$\begin{aligned} H_{\mathcal{L}_1}(0, \beta_1^I, \beta_2^I) &= \begin{pmatrix} \frac{1}{250}(13\sqrt{6}-42) & 0 & 0 \\ 0 & \frac{1}{100}(23\sqrt{6}-32) & \frac{1}{50}(8+13\sqrt{6}) \\ 0 & \frac{1}{50}(8+13\sqrt{6}) & \frac{1}{5}(\sqrt{6}-4) \end{pmatrix} \\ H_{\mathcal{L}_1}(0, \beta_1^{II}, \beta_2^{II}) &= \begin{pmatrix} \frac{1}{250}(-42-13\sqrt{6}) & 0 & 0 \\ 0 & \frac{1}{100}(-32-23\sqrt{6}) & \frac{1}{50}(8-13\sqrt{6}) \\ 0 & \frac{1}{50}(8-13\sqrt{6}) & \frac{1}{5}(-4-\sqrt{6}) \end{pmatrix} \\ H_{\mathcal{L}_1}(0, \beta_1^{III}, \beta_2^{III}) &= \begin{pmatrix} \frac{1}{4}(7-3\sqrt{5}) & 0 & 0 \\ 0 & \frac{1}{2}(\sqrt{5}-3) & \frac{1}{4}(-1-\sqrt{5}) \\ 0 & \frac{1}{4}(-1-\sqrt{5}) & \frac{1}{4}(\sqrt{5}-1) \end{pmatrix}. \end{aligned}$$

From Sylvester’s criterion, we conclude that

$$\begin{cases} \mathcal{L}_1(0, \beta_1^{III}, \beta_2^{III}) = \frac{1}{4} - \text{saddle point} \\ \mathcal{L}_1(0, \beta_1^I, \beta_2^I) = \frac{3}{50}(9-\sqrt{6}) \approx 0.393 - \text{saddle point} \\ \mathcal{L}_1(0, \beta_1^{II}, \beta_2^{II}) = \frac{3}{50}(9+\sqrt{6}) \approx 0.687 - \text{global maximum} \end{cases}$$

□

Next, consider parameterization YZY of the first coherent evolution and ZYZ of the second coherent evolution to find the critical points on $(\mathcal{B} \setminus \{\mathbb{I}\}) \times (\mathcal{R} \setminus \mathcal{B})$. Likewise, we obtain a matrix representation of unitary evolution, from which the transition probability will be

$$\begin{aligned} P_{1 \rightarrow 2}(c_1, \mathcal{M}_{|1\rangle\langle 1|}, c_2) &= \frac{1}{4} \sin^2 \beta_2 \left[1 + \left(\cos \alpha_1 \cos \gamma_1 - \cos \beta_1 \sin \alpha_1 \sin \gamma_1 \right)^2 \right] \\ &+ \frac{1}{8} \cos^2 \beta_2 \left[4 \cos^2 \alpha_1 \sin^2 \gamma_1 + \sin^2 \alpha_1 (3 + \cos 2\gamma_1 - 2 \cos 2\beta_1 \sin^2 \gamma_1) \right] \\ &+ 2 \cos \beta_1 \sin 2\alpha_1 \sin 2\gamma_1 + \text{Re} \left[e^{i(\beta_1-\gamma_2)} \cos \beta_2 \sin \beta_2 \left(\cos \frac{\gamma_1}{2} \sin \frac{\alpha_1}{2} + e^{-i\beta_1} \cos \frac{\alpha_1}{2} \sin \frac{\gamma_1}{2} \right)^2 \right] \\ &\times \left(-e^{-i\beta_1} \cos^2 \frac{\gamma_1}{2} \sin \alpha_1 + e^{i\beta_1} \sin \alpha_1 \sin^2 \frac{\gamma_1}{2} - \cos \alpha_1 \sin \gamma_1 \right) =: \mathcal{L}_2(\alpha_1, \beta_1, \gamma_1, \beta_2, \gamma_2) \equiv \mathcal{L}_2, \end{aligned}$$

where $(\alpha_i, \beta_i, \gamma_i) \in (-\pi, \pi] \times (0, \pi) \times (-\pi, \pi]$, $i = 1, 2$. Our set $(\mathcal{B} \setminus \{\mathbb{I}\}) \times (\mathcal{R} \setminus \mathcal{B})$ corresponds to $\alpha_1 = \gamma_1 = 0$.

Lemma 2. All critical points of $\mathcal{L}_2(\alpha_1, \beta_1, \gamma_1, \beta_2, \gamma_2)$ on the surface $\alpha_1 = \gamma_1 = 0$, their types and the corresponding values of the function are given in Table 2.

Table 2. Critical points, their types and values of the objective function $\mathfrak{L}_2(\alpha_1, \beta_1, \gamma_1, \beta_2, \gamma_2)$.

$(\alpha_1, \beta_1, \gamma_1, \beta_2, \gamma_2)$	$P_{1 \rightarrow 2}$	Type of Point
$(0, \beta_1, 0, \frac{\pi}{2}, \gamma_2), \beta_1 \in (0, \pi), \gamma_2 \in (-\pi, \pi]$	1/2	Second-order trap

Proof.

$$\begin{cases} (\mathfrak{L}_2)'_{\alpha_1}|_{\alpha_1, \gamma_1=0} = 0 \\ (\mathfrak{L}_2)'_{\beta_1}|_{\alpha_1, \gamma_1=0} = 0 \\ (\mathfrak{L}_2)'_{\gamma_1}|_{\alpha_1, \gamma_1=0} = 0 \\ (\mathfrak{L}_2)'_{\beta_2}|_{\alpha_1, \gamma_1=0} = \cos \beta_2 \sin \beta_2 \\ (\mathfrak{L}_2)'_{\gamma_2}|_{\alpha_1, \gamma_1=0} = 0 \end{cases} .$$

Thus, from the condition $\nabla \mathfrak{L}_2 = 0$, we have the following critical points $(0, \beta_1, 0, \frac{\pi}{2}, \gamma_2)$. The Hessian matrix at the corresponding points is

$$H_{\mathfrak{L}_2} = \begin{pmatrix} -\frac{1}{2} & 0 & -\frac{1}{2} \cos \beta_1 & 0 & 0 \\ 0 & 0 & 0 & 0 & 0 \\ -\frac{1}{2} \cos \beta_1 & 0 & -\frac{1}{2} & 0 & 0 \\ 0 & 0 & 0 & -1 & 0 \\ 0 & 0 & 0 & 0 & 0 \end{pmatrix} .$$

Since the eigenvalues are $(0, 0, -1, -\frac{1}{2}(1 + \cos \beta_1), -\frac{1}{2}(1 - \cos \beta_1))$, we conclude that $(0, \beta_1, 0, \frac{\pi}{2}, \gamma_2)$ is a second-order trap. \square

Next, consider parameterization YZY of the second coherent evolution and ZYZ of the first coherent evolution to find the critical points on $(\mathcal{R} \setminus \mathcal{B}) \times (\mathcal{B} \setminus \{\mathbb{I}\})$. Likewise, we obtain a matrix representation of unitary evolution, from which the transition probability will be

$$\begin{aligned} P_{1 \rightarrow 2}(c_1, \mathcal{M}_{|1\rangle\langle 1|}, c_2) &= \frac{1}{2} \sin^2 \beta_1 (\cos \alpha_2 \cos \gamma_2 - \cos \beta_2 \sin \alpha_2 \sin \gamma_2)^2 \\ &+ \frac{1}{8} (3 + \cos 2\beta_1) [\sin \beta_2 (\cos \beta_2 \cos \gamma_2 \sin 2\alpha_2 + \cos^2 \alpha_2 \sin \gamma_2) \\ &+ \frac{1}{4} \sin^2 \alpha_2 (3 + \cos 2\gamma_2 - 2 \cos 2\beta_2 \sin^2 \gamma_2)] + \sin \beta_1 \sin^2 \frac{\beta_1}{2} (\cos \alpha_2 \cos \gamma_2 - \cos \beta_2 \sin \alpha_2 \sin \gamma_2) \\ &\times [\sin \alpha_2 \cos (\alpha_1 - \beta_2) \sin^2 \frac{\gamma_2}{2} - \cos \alpha_1 \cos \alpha_2 \sin \gamma_2 - \cos (\alpha_1 + \beta_2) \cos^2 \frac{\gamma_2}{2} \sin \alpha_2] \\ &=: \mathfrak{L}_3(\alpha_1, \beta_1, \alpha_2, \beta_2, \gamma_2) \equiv \mathfrak{L}_3, \end{aligned}$$

where $(\alpha_i, \beta_i, \gamma_i) \in (-\pi, \pi] \times (0, \pi) \times (-\pi, \pi], i = 1, 2$. The set $(\mathcal{R} \setminus \mathcal{B}) \times (\mathcal{B} \setminus \{\mathbb{I}\})$ corresponds to $\alpha_2 = \gamma_2 = 0$.

Lemma 3. *There are no critical points of $\mathfrak{L}_3(\alpha_1, \beta_1, \alpha_2, \beta_2, \gamma_2)$ on the surface $\alpha_2 = \gamma_2 = 0$.*

Proof.

$$\begin{cases} (\mathfrak{L}_3)'_{\alpha_2}|_{\alpha_2, \gamma_2=0} = -\cos (\alpha_1 + \beta_2) \sin^2 \frac{\beta_1}{2} \sin \beta_1 \\ (\mathfrak{L}_3)'_{\beta_2}|_{\alpha_2, \gamma_2=0} = 0 \\ (\mathfrak{L}_3)'_{\gamma_2}|_{\alpha_2, \gamma_2=0} = -\cos \alpha_1 \sin^2 \frac{\beta_1}{2} \sin \beta_1 \\ (\mathfrak{L}_3)'_{\alpha_1}|_{\alpha_2, \gamma_2=0} = 0 \\ (\mathfrak{L}_3)'_{\beta_1}|_{\alpha_2, \gamma_2=0} = \cos \beta_1 \sin \beta_1 \end{cases} .$$

Thus, from the condition $\nabla \mathfrak{L}_3 = 0$, we see that there are no critical points on the considered domain. \square

Finally, consider parameterization YZY of both the first and second coherent evolutions to find the critical points on $(\mathcal{B} \setminus \{\mathbb{I}\}) \times (\mathcal{B} \setminus \{\mathbb{I}\})$. We will not provide the expression for $P_{1 \rightarrow 2}(c_1, \mathcal{M}_{|1\rangle\langle 1|}, c_2) = \mathfrak{L}_4(\alpha_1, \beta_1, \gamma_1, \alpha_2, \beta_2, \gamma_2) = \mathfrak{L}_4$ in this parameterization, since we are only interested in the critical points and functional values on the surface $\alpha_1 = \gamma_1 = \alpha_2 = \gamma_2 = 0$ (corresponding to $(\mathcal{B} \setminus \{\mathbb{I}\}) \times (\mathcal{B} \setminus \{\mathbb{I}\})$).

Lemma 4. All critical points of $\mathfrak{L}_4(\alpha_1, \beta_1, \gamma_1, \alpha_2, \beta_2, \gamma_2)$ on the surface $\alpha_1 = \gamma_1 = \alpha_2 = \gamma_2 = 0$, their types and the corresponding values of the function are given in Table 3.

Table 3. Critical points, their types and values of the objective function $\mathfrak{L}_4(\alpha_1, \beta_1, \gamma_1, \alpha_2, \beta_2, \gamma_2)$.

$(\alpha_1, \beta_1, \gamma_1, \alpha_2, \beta_2, \gamma_2)$	$P_{1 \rightarrow 2}$	Type of Point
$(0, \beta_1, 0, 0, \beta_2, 0),$ $\beta_1, \beta_2 \in (0, \pi)$	0	Global minima

Proof. One can easily notice that $\nabla \mathfrak{L}_4|_{\alpha_1=\gamma_1=\alpha_2=\gamma_2=0} = 0$, so $(0, \beta_1, 0, 0, \beta_2, 0)$ are critical points for every $\beta_1, \beta_2 \in (0, \pi)$.

The Hessian matrix at the corresponding points is

$$H_{\mathfrak{L}_4} = \begin{pmatrix} 1 & 0 & \cos \beta_1 & 0 & 0 & 0 \\ 0 & 0 & 0 & 0 & 0 & 0 \\ \cos \beta_1 & 0 & 1 & 0 & 0 & 0 \\ 0 & 0 & 0 & 1 & 0 & \cos \beta_2 \\ 0 & 0 & 0 & 0 & 0 & 0 \\ 0 & 0 & 0 & \cos \beta_2 & 0 & 1 \end{pmatrix}.$$

Its eigenvalues are $(0, 0, 1 + \cos \beta_1, 1 - \cos \beta_1, 1 + \cos \beta_2, 1 - \cos \beta_2)$. Since $\mathfrak{L}_4(0, \beta_1, 0, 0, \beta_2, 0) = 0$, points $(0, \beta_1, 0, 0, \beta_2, 0)$ are global minima for every $\beta_1, \beta_2 \in (0, \pi)$. \square

It remains for us to study $\{\mathbb{I}\} \times \{\mathbb{I}\}, \{\mathbb{I}\} \times (\mathcal{R} \setminus \{\mathbb{I}\}), (\mathcal{R} \setminus \{\mathbb{I}\}) \times \{\mathbb{I}\}$. Obviously, $\{\mathbb{I}\} \times \{\mathbb{I}\}$ is a global minimum with $P_{1 \rightarrow 2}(\mathbb{I}, \mathcal{M}_{|1\rangle\langle 1|}, \mathbb{I}) = 0$, and $\{\mathbb{I}\} \times (\mathcal{R} \setminus \{\mathbb{I}\})$ determines the same functional as $(\mathcal{R} \setminus \{\mathbb{I}\}) \times \{\mathbb{I}\}$, i.e. $P_{1 \rightarrow 2}(\mathbb{I}, \mathcal{M}_{|1\rangle\langle 1|}, U) = P_{1 \rightarrow 2}(U, \mathcal{M}_{|1\rangle\langle 1|}, \mathbb{I})$.

Consider $\{\mathbb{I}\} \times (\mathcal{R} \setminus \mathcal{B})$. We use YZY representation to parameterize this set. The objective function has the following form:

$$P_{1 \rightarrow 2}(\mathbb{I}, \mathcal{M}_{|1\rangle\langle 1|}, c) = \frac{1}{2} \sin^2 \beta =: \mathfrak{L}_5(\beta), \tag{23}$$

where $\beta \in (0, \pi)$. From the simplicity of $\mathfrak{L}_5(\beta)$, the following lemma obviously follows.

Lemma 5. All critical points of $\mathfrak{L}_5(\beta)$, their types and the corresponding values of the function are given in Table 4.

Table 4. Critical points, their types and values of the objective function $\mathfrak{L}_5(\beta)$.

β	$P_{1 \rightarrow 2}$	Type of Point
$\pi/2$	1/2	Second-order trap

Consider $\{\mathbb{I}\} \times (\mathcal{B} \setminus \{\mathbb{I}\})$. We use YZY representation to parameterize this set. The objective function has the following form:

$$P_{1 \rightarrow 2}(\mathbb{I}, \mathcal{M}_{|1\rangle\langle 1|}, c) = \frac{1}{2} \left(\cos^4 \frac{\gamma}{2} \sin^2 \alpha + \sin^2 \alpha \sin^4 \frac{\gamma}{2} \sin^2 \alpha + \cos^2 \alpha \sin^2 \gamma \right) + \frac{1}{4} \left(\frac{1}{2} \cos \beta \sin 2\alpha \sin 2\gamma - \cos 2\beta \sin^2 \gamma \sin^2 \alpha \right) =: \mathfrak{L}_6(\alpha, \beta, \gamma),$$

Lemma 6. All critical points of $\mathcal{L}_6(\alpha, \beta, \gamma)$ on the surface $\alpha = \gamma = 0$ and corresponding values are given in Table 5.

Table 5. Critical points, their types and values of the objective function $\mathcal{L}_6(\alpha, \beta, \gamma)$.

(α, β, γ)	$P_{1 \rightarrow 2}$	Type of Point
$(0, \beta, 0), \beta \in (0, \pi)$	1/2	Second-order trap

Proof. Since $\nabla \mathcal{L}_6(0, \beta, 0) = 0$, points $(0, \beta, 0)$ are critical for every $\beta \in (0, \pi)$. The Hessian matrix at the corresponding points is

$$H_{\mathcal{L}_6} = \begin{pmatrix} 1 & 0 & \cos \beta \\ 0 & 0 & 0 \\ \cos \beta & 0 & 1 \end{pmatrix}.$$

From Sylvester’s criterion, we conclude that $(0, \beta, 0)$ is a second-order trap. □

Remark 1. The types of critical points of $P_{1 \rightarrow 2}(U(1), \mathcal{M}_{|1\rangle\langle 1|}, U(2))$ are the same as for $\mathcal{L}_1, \mathcal{L}_2, \mathcal{L}_3, \mathcal{L}_4, \mathcal{L}_5, \mathcal{L}_6$ (Table 6).

Theorem 1. All the critical points of the kinematic control landscape of the transition probability $P_{1 \rightarrow 2}(U(1), \mathcal{M}_{|1\rangle\langle 1|}, U(2))$ are global minima, saddles, second-order traps or global maxima.

Table 6. Critical points, their types and values of the objective function. Asterisk indicates that the corresponding variable can take any value in its range.

$(U(1), U(2)) : (\alpha_1, \beta_1, \gamma_1, \alpha_2, \beta_2, \gamma_2)$	$P_{1 \rightarrow 2}$	Type of Point
$(YZY, YZY) : (0, \beta_1^*, 0, 0, \beta_2^*, 0)$	0	Global minima
$(\mathbb{I}, \mathbb{I}) : (0, 0, 0, 0, 0, 0)$	0	Global minima
$(ZYZ, ZYZ) : (\alpha_1^*, \frac{\pi}{2}, \gamma_1^*, \alpha_2^*, \frac{\pi}{2}, \pm \frac{\pi}{2} - \alpha_1^*)$	1/4	Saddle point
$(ZYZ, ZYZ) : (\alpha_1^*, \arccos(\frac{-1+\sqrt{5}}{2}), \gamma_1^*, \alpha_2^*, \pi - \frac{1}{2} \arctan(2\sqrt{2 + \sqrt{5}}), \pi - \alpha_1^*)$	1/4	Saddle point
$(ZYZ, ZYZ) : (\alpha_1^*, \arccos(\frac{-1+\sqrt{5}}{2}), \gamma_1^*, \alpha_2^*, \frac{1}{2} \arctan(2\sqrt{2 + \sqrt{5}}), -\alpha_1^*)$	1/4	Saddle point
$(ZYZ, ZYZ) : (\alpha_1^*, \arccos(\frac{1+\sqrt{6}}{5}), \gamma_1^*, \alpha_2^*, \frac{1}{2} \arccos(\frac{1}{1-\sqrt{6}}), \pi - \alpha_1^*)$	$\frac{3}{50}(9 - \sqrt{6})$	Saddle point
$(ZYZ, ZYZ) : (\alpha_1^*, \arccos(\frac{1+\sqrt{6}}{5}), \gamma_1^*, \alpha_2^*, \pi - \frac{1}{2} \arccos(\frac{1}{1-\sqrt{6}}), -\alpha_1^*)$	$\frac{3}{50}(9 - \sqrt{6})$	Saddle point
$(YZY, YZY) : (0, \beta_1^*, 0, \alpha_2^*, \frac{\pi}{2}, \gamma_2^*)$	1/2	Second-order trap
$(\mathbb{I}, YZY) : (0, 0, 0, 0, \frac{\pi}{2}, 0)$	1/2	Second-order trap
$(\mathbb{I}, YZY) : (0, 0, 0, 0, \beta_2^*, 0)$	1/2	Second-order trap
$(ZYZ, \mathbb{I}) : (0, \frac{\pi}{2}, 0, 0, 0, 0)$	1/2	Second-order trap
$(YZY, \mathbb{I}) : (0, \beta_1^*, 0, 0, 0, 0)$	1/2	Second-order trap
$(ZYZ, ZYZ) : (\alpha_1^*, \arccos(\frac{1-\sqrt{6}}{5}), \gamma_1^*, \alpha_2^*, \frac{1}{2} \arccos(\frac{1}{1+\sqrt{6}}), \pi - \alpha_1^*)$	$\frac{3}{50}(9 + \sqrt{6})$	Global maxima
$(ZYZ, ZYZ) : (\alpha_1^*, \arccos(\frac{1-\sqrt{6}}{5}), \gamma_1^*, \alpha_2^*, \pi - \frac{1}{2} \arccos(\frac{1}{1+\sqrt{6}}), -\alpha_1^*)$	$\frac{3}{50}(9 + \sqrt{6})$	Global maxima

Corollary 1. One has

$$\max_{c_1, c_2} P_{1 \rightarrow 2}(c_1, \mathcal{M}_{|1\rangle\langle 1|}, c_2) = \frac{3}{50}(9 + \sqrt{6}). \tag{24}$$

One can check that the expression on the right-hand side (r.h.s.) of (24) coincides with the r.h.s. of (18).

7. Comparison with other Cases of Measurement-Assisted Transition Probabilities

Here, for comparison, we study other cases of transition probabilities.

Theorem 2. *One has*

$$\max_{c_1, c_2} P_{1 \rightarrow 3}(c_1, \mathcal{M}_{|1\rangle\langle 1|}, c_2) = 1 \tag{25}$$

$$\max_{c_1, c_2} P_{1 \rightarrow 3}(c_1, \mathcal{M}_{|2\rangle\langle 2|}, c_2) = 1. \tag{26}$$

Proof. Here, there is no need to compute $P_{1 \rightarrow 3}$ explicitly using Euler parameterization. Notice that

$$\langle 3 | \rho(0-) | 3 \rangle = \langle 3 | U(1) | 1 \rangle \langle 1 | U^\dagger(1) | 3 \rangle = |\langle 3 | U(1) | 1 \rangle|^2 = \sin^4 \frac{\beta_1}{2}.$$

Since we can set $\alpha_2 = \beta_2 = \gamma_2 = 0$ (second evolution is trivial) and, after measurement, we have $\langle 3 | \rho(0+) | 3 \rangle = \langle 3 | \rho(0-) | 3 \rangle$, we obtain

$$\max_{c_1, c_2} P_{1 \rightarrow 3}(c_1, \mathcal{M}_{|1\rangle\langle 1|}, c_2) = \max_{\alpha_1, \beta_1, \gamma_1 \in [0, 2\pi]} \langle 3 | \rho(0-) | 3 \rangle = \max_{\beta_1 \in [0, 2\pi]} \sin^4 \frac{\beta_1}{2} = 1.$$

Similarly, we obtain

$$\max_{c_1, c_2} P_{1 \rightarrow 3}(c_1, \mathcal{M}_{|2\rangle\langle 2|}, c_2) = \max_{\alpha_1, \beta_1, \gamma_1 \in [0, 2\pi]} \langle 3 | \rho(0-) | 3 \rangle = \max_{\beta_1 \in [0, 2\pi]} \sin^4 \frac{\beta_1}{2} = 1.$$

□

Theorem 3. *One has*

$$\max_{c_1, c_2} P_{1 \rightarrow 2}(c_1, \mathcal{M}_{|2\rangle\langle 2|}, c_2) = \frac{1}{2}.$$

Proof. From (15), we obtain

$$\begin{aligned} \langle 2 | \rho(T_2) | 2 \rangle &= |U_{11}(1)|^2 |U_{21}(2)|^2 + |U_{21}(1)|^2 |U_{22}(2)|^2 + |U_{31}(1)|^2 |U_{23}(2)|^2 \\ &\quad + 2\text{Re}[U_{11}(1)\overline{U_{31}(1)}U_{22}(2)\overline{U_{23}(2)}]. \end{aligned}$$

Computing the transition probability gives

$$\begin{aligned} P_{1 \rightarrow 2}(c_1, \mathcal{M}_{|2\rangle\langle 2|}, c_2) &= \langle 2 | \rho(T_2) | 2 \rangle \\ &= \frac{1}{2} \cos^2 \beta_2 \sin^2 \beta_1 + \frac{1}{8} (3 + \cos 2\beta_1) \sin^2 \beta_2 + \frac{1}{4} \sin^2 \beta_1 \sin^2 \beta_2 \\ &= \frac{1}{2} (\sin^2 \beta_1 + \sin^2 \beta_2 + \sin^2 \beta_1 \sin^2 \beta_2) \equiv \mathfrak{M}(\beta_1, \beta_2). \end{aligned}$$

In this case, the transition probability is a function of only two kinematic controls, β_1 and β_2 . Notice that $\mathfrak{M}(\beta_1, \beta_2) \leq 1/2$ and $\mathfrak{M}(0, \pi/2) = 1/2$. Thus,

$$\max_{c_1, c_2} P_{1 \rightarrow 2}(c_1, \mathcal{M}_{|2\rangle\langle 2|}, c_2) = \frac{1}{2}.$$

□

8. Discussion

In this work, we considered a three-level quantum system with dynamical symmetry that is controlled by using coherent control assisted by the back-action of the non-selective quantum measurement of the population of some state. In the absence of the measurement, only 1/2 of the population can be transferred from the ground to the intermediate state. Maximum measurement-assisted transition from the ground to the intermediate state was computed before. In the kinematic representation of the dynamics, the controls are Euler angles parameterizing the spin-1 representation of the Lie algebra $\mathfrak{su}(2)$. We studied in

detail the kinematic control landscape of the transition probability from the ground to the intermediate state, describing all its critical points. We find that all critical points of the kinematic control landscape are global maxima, global minima, second-order traps or saddles. For comparison, we studied the transition probability between the ground and highest excited states, as well as the case when both these transition probabilities are assisted by incoherent control implemented through the measurement of the intermediate state. The next important question is what types of critical points are present in the dynamic control landscape. Let $F_{\text{dyn}} : L^2 \rightarrow \mathcal{R}$ be the mapping that maps any control $f \in L^2$ into the corresponding evolution operator $U_T^f \in \mathcal{R}$ with some fixed, sufficiently large T . Let $P_{1 \rightarrow 2}^{\text{kin}} : \mathcal{R} \times \mathcal{R} \rightarrow [0, 1]$ be the kinematic transition probability (defined by Equation (16)). The dynamic landscape represents the transition probability as a function of two coherent controls, f_1 and f_2 (defined by Equation (8)), and can be considered as a composition of the mappings F_{dyn} and $P_{1 \rightarrow 2}^{\text{kin}}$ as $P_{1 \rightarrow 2}(f_1, f_2) = P_{\text{kin}} \circ (F_{\text{dyn}} \times F_{\text{dyn}})$. At so-called regular points, where the Jacobian of the map $F_{\text{dyn}} \times F_{\text{dyn}}$ from the control space to $\mathcal{R} \times \mathcal{R}$ has full rank, the structure of the dynamical control landscape is the same as the structure of the kinematic control landscape (see Theorem 1 in [71]). Thus, our finding implies that at regular points, the dynamic landscape has the same points as the kinematic landscape. However, at singular points, where the Jacobian is rank-deficient, the situation can be different. Thus, our results do not exclude the existence of other critical points in the dynamic landscape as well. Finding such points and establishing the control landscape structure around them is an important problem that requires a special analysis beyond this work.

Author Contributions: Conceptualization, A.P.; methodology, A.P. and M.E.; formal analysis, M.E.; writing, A.P. and M.E.; visualization, M.E.; supervision, A.P.; discussion, A.P. All authors have read and agreed to the published version of the manuscript.

Funding: This work is supported by the Russian Science Foundation under grant № 22-11-00330, <https://rscf.ru/en/project/22-11-00330/> (accessed on 5 May 2023) and was performed at Steklov Mathematical Institute of Russian Academy of Sciences.

Data Availability Statement: Not applicable.

Acknowledgments: We thank B.O. Volkov, V.N. Petruhanov and S.A. Kuznetsov for useful comments.

Conflicts of Interest: The authors declare no conflicts of interest.

References

1. Koch, C.; Boscain, U.; Calarco, T.; Dirr, G.; Filipp, S.; Glaser, S.; Kosloff, R.; Montangero, S.; Schulte-Herbrüggen, T.; Sugny, D.; et al. Quantum optimal control in quantum technologies. Strategic report on current status, visions and goals for research in Europe. *EPJ Quantum Technol.* **2022**, *9*, 19. [[CrossRef](#)]
2. Rice, S.; Zhao, M. *Modern Quantum Mechanics*; John Wiley & Sons, Inc.: New York, NY, USA, 2000.
3. Tannor, D. *Introduction to Quantum Mechanics: A Time-Dependent Perspective*; Univ. Science Books: Sausalito, CA, USA, 2007.
4. Shapiro, M.; Brumer, P. *Quantum Control of Molecular Processes. Second, Revised and Enlarged Edition*; WILEY-VCH Verlag GmbH & Co. KGaA: Weinheim, Germany, 2012.
5. Pechen, A.; Il'in, N.; Shuang, F.; Rabitz, H. Quantum control by von Neumann measurements. *Phys. Rev. A* **2006**, *74*, 052102. [[CrossRef](#)]
6. Shuang, F.; Zhou, M.; Pechen, A.; Wu, R.; Shir, O.; Rabitz, H. Control of quantum dynamics by optimized measurements. *Phys. Rev. A* **2008**, *78*, 063422. [[CrossRef](#)]
7. Dong, D.Y.; Chen, C.L.; Tarn, T.J.; Pechen, A.; Rabitz, H. Incoherent control of quantum systems with wavefunction controllable subspaces via quantum reinforcement learning. *IEEE Trans. Syst. Man Cybern. Part Cybern.* **2008**, *38*, 957–962. [[CrossRef](#)]
8. Sugny, D.; Kontz, C. Optimal control of a three-level quantum system by laser fields plus von Neumann measurements. *Phys. Rev. A* **2008**, *77*, 063420. [[CrossRef](#)]
9. Blok, M.; Bonato, C.; Markham, M.; Twitchen, D.; Dobrovitski, V.; Hanson, R. Manipulating a qubit through the backaction of sequential partial measurements and real-time feedback. *Nat. Phys.* **2014**, *10*, 189–193. [[CrossRef](#)]
10. Lucas, F.; Hornberger, K. Incoherent control of the retinal isomerization in rhodopsin. *Phys. Rev. Lett.* **2014**, *113*, 058301. [[CrossRef](#)]
11. Pechen, A.N.; Trushechkin, A.S. Measurement-assisted Landau-Zener transitions. *Phys. Rev. A* **2015**, *91*, 052316. [[CrossRef](#)]

12. Zhang, P.; Ai, Q.; Li, Y.; Xu, D.; Sun, C. Dynamics of quantum Zeno and anti-Zeno effects in an open system. *Sci. China Phys. Mech. Astron.* **2014**, *57*, 194–207. [[CrossRef](#)]
13. Qi, H.; Mu, B.; Petersen, I.R.; Shi, G. Measurement-induced boolean dynamics for open quantum networks. *IEEE Trans. Control. Netw. Syst.* **2023**, *10*, 134–146. [[CrossRef](#)]
14. Kumar, P.; Snizhko, K.; Gefen, Y.; Rosenow, B. Optimized steering: Quantum state engineering and exceptional points. *Phys. Rev. A* **2022**, *105*, L010203. [[CrossRef](#)]
15. Hacoheh-Gourgy, S.; García-Pintos, L.P.; Martin, L.S.; Dressel, J.; Siddiqi, I. Incoherent qubit control using the quantum Zeno effect. *Phys. Rev. Lett.* **2018**, *120*, 020505. [[CrossRef](#)] [[PubMed](#)]
16. Cejnar, P.; Stránský, P.; Střeleček, J.; Matus, F. Decoherence-assisted quantum driving. *Phys. Rev. A* **2023**, *107*, L030603. [[CrossRef](#)]
17. Kozyrev, S.V.; Pechen, A.N. Quantum feedback control in quantum photosynthesis. *Phys. Rev. A* **2022**, *106*, 032218. [[CrossRef](#)]
18. Harraz, S.; Yang, J.; Li, K.; Cong, S. Quantum state transfer control based on the optimal measurement. *Optim. Control. Appl. Methods* **2017**, *38*, 744–753. doi: 10.1002/oca.2287. [[CrossRef](#)]
19. Onofrio, R.; Viola, L. Quantum damping of position due to energy measurements. *Phys. Rev. A* **1996**, *53*, 3773–3780. [[CrossRef](#)]
20. Viola, L.; Onofrio, R. Measured quantum dynamics of a trapped ion. *Phys. Rev. A* **1997**, *55*, R3291–R3294. *PhysRevA*.55.R3291. [[CrossRef](#)]
21. Roa, L.; Delgado, A.; Ladrón De Guevara, M.L.; Klimov, A.B. Measurement-driven quantum evolution. *Phys. Rev. A* **2006**, *73*, 012322. [[CrossRef](#)]
22. Harrington, P.M.; Monroe, J.T.; Murch, K.W. Quantum Zeno effects from measurement controlled qubit-bath interactions. *Phys. Rev. Lett.* **2017**, *118*, 240401. [[CrossRef](#)]
23. Dajka, J. Scattering-like control of the Cheshire Cat effect in open quantum systems. *Quantum Rep.* **2019**, *2*, 1–11. [[CrossRef](#)]
24. Gangat, A.A.; Milburn, G.J. Quantum clocks driven by measurement. *arXiv* **2021**. [[CrossRef](#)]
25. Blumenthal, E.; Mor, C.; Dinger, A.A.; Martin, L.S.; Lewalle, P.; Burgarth, D.; Whaley, K.B.; Hacoheh-Gourgy, S. Demonstration of universal control between non-interacting qubits using the quantum Zeno effect. *NPJ Quantum Inf.* **2022**, *8*, 88. [[CrossRef](#)]
26. Lewalle, P.; Martin, L. S.; Flurin, E.; Zhang, S.; Blumenthal, E.; Hacoheh-Gourgy, S.; Burgarth, D.; Whaley, K.B. A Multi-qubit quantum gate using the Zeno effect. *arXiv* **2022**. [[CrossRef](#)]
27. Borah, S.; Sarma, B.; Kewming, M.; Quijandria, F.; Milburn, G.J.; Twamley, J. Measurement-based estimator scheme for continuous quantum error correction. *Phys. Rev. Res.* **2022**, *4*, 033207. [[CrossRef](#)]
28. Perret, A.; Bérubé-Lauzière, Y. Preparation of cavity Fock state superpositions by reinforcement learning exploiting measurement back-action. *arXiv* **2023**. [[CrossRef](#)]
29. Clausen, H.G.; Rahman, S.A.; Karabacak, Ö.; Wisniewski, R. Measurement-based control for minimizing energy functions in quantum systems. *arXiv* **2023**. [[CrossRef](#)]
30. Mukhamedov, F.; Qaralleh, I. Controlling problem within a class of two-level positive maps. *Symmetry* **2022**, *14*, 2280. [[CrossRef](#)]
31. Piacentini, F.; Avella, A.; Rebufello, E.; Lussana, R.; Villa, F.; Tosi, A.; Gramegna, M.; Brida, G.; Cohen, E.; Vaidman, L.; et al. Determining the quantum expectation value by measuring a single photon. *Nat. Phys.* **2017**, *13*, 1191–1194. *nphys4223*. [[CrossRef](#)]
32. Rabitz, H.A.; Hsieh, M.M.; Rosenthal, C.M. Quantum optimally controlled transition landscapes. *Science* **2004**, *303*, 1998–2001. [[CrossRef](#)]
33. de Fouquieres, P.; Schirmer, S.G. Are there traps in quantum control landscapes? *Phys. Rev. Lett.* **2011**, *106*, 120402. [[CrossRef](#)]
34. de Fouquieres, P.; Schirmer, S.G. A closer look at quantum control landscapes and their implication for control optimization. *Infim. Dimens. Anal. Quant. Probab. Rel. Top.* **2013**, *16*, 1350021. [[CrossRef](#)]
35. Volkov, B.; Pechen, A. High-order traps in quantum control problems for certain strongly degenerate systems. *Uspekhi Mat. Nauk.* **2023**, *78*, 191–192. [[CrossRef](#)]
36. Pechen, A.; Brif, C.; Wu, R.; Chakrabarti, R.; Rabitz, H. General unifying features of controlled quantum phenomena. *Phys. Rev. A* **2010**, *82*, 030101. [[CrossRef](#)]
37. Pechen, A.; Rabitz, H. Unified analysis of terminal-time control in classical and quantum systems. *Europhys. Lett.* **2010**, *91*, 60005. [[CrossRef](#)]
38. Moore, K.W.; Pechen, A.; Feng, X.J.; Dominy, J.; Beltrani, V.; Rabitz, H. Universal characteristics of chemical synthesis and property optimization. *Chem. Sci.* **2011**, *2*, 417–424. [[CrossRef](#)]
39. Moore, K.W.; Pechen, A.; Feng, X.J.; Dominy, J.; Beltrani, V.J.; Rabitz, H. Why is chemical synthesis and property optimization easier than expected? *Phys. Chem. Chem. Phys.* **2011**, *13*, 10048–10070. [[CrossRef](#)]
40. Hioe, F.T. Dynamic symmetries in quantum electronics. *Phys. Rev. A* **1983**, *28*, 879–886. [[CrossRef](#)]
41. Turinici, G.; Rabitz, H. Quantum wavefunction controllability. *Chem. Phys.* **2001**, *267*, 1–9. [[CrossRef](#)]
42. Engelhardt, G.; Cao, J. Dynamical symmetries of periodically-driven quantum systems and their spectroscopic signatures. *Phys. Rev. Lett.* **2020**, *126*, 090601. [[CrossRef](#)]
43. Lüders, G. Über die Zustandsänderung durch den Meßprozeß. *Ann. Phys.* **1951**, *8*, 322. Translation to English with discussion: K.A. Kirkpatrick, *Ann. Phys.* **2006**, *15*, 663–670. [[CrossRef](#)]
44. von Neumann, J. *Mathematical Foundations of Quantum Mechanics*; Princeton University Press: Princeton, NJ, USA, 1955.
45. Wiseman, H.W.; Milburn, G.J. *Quantum Measurement and Control*; Cambridge University Press: Cambridge, UK, 2014. [[CrossRef](#)]
46. Wiseman, H.M.; Milburn, G.J. Quantum theory of optical feedback via homodyne detection. *Phys. Rev. Lett.* **1993**, *70*, 548–551. [[CrossRef](#)]

47. Wiseman, H.M. Quantum theory of continuous feedback. *Phys. Rev. A* **1994**, *49*, 2133–2150. PhysRevA.49.2133. [[CrossRef](#)] [[PubMed](#)]
48. Lloyd, S. Coherent quantum feedback. *Phys. Rev. A* **2000**, *62*, 022108. [[CrossRef](#)]
49. Doherty, A.C.; Habib, S.; Jacobs, K.; Mabuchi, H.; Tan, S.M. Quantum feedback control and classical control theory. *Phys. Rev. A* **2000**, *62*, 012105. [[CrossRef](#)]
50. Gough J.; Belavkin V. P.; Smolyanov, O.G. Hamilton–Jacobi–Bellman equations for quantum optimal feedback control. *J. Opt. B Quantum Semiclass. Opt.* **2005**, *7*, S237–S244. [[CrossRef](#)]
51. Lloyd, S.; Viola, L. Engineering quantum dynamics. *Phys. Rev. A* **2001**, *65*, 010101. [[CrossRef](#)]
52. Rossi, M.; Mason, D.; Chen, J.; Tsaturyan, Y.; Schliesser, A. Measurement-based quantum control of mechanical motion. *Nature* **2018**, *563*, 53–58. [[CrossRef](#)]
53. Schirmer, S.G.; Jonckheere, E.A.; Langbein, F.C. Design of feedback control laws for information transfer in spintronics networks. *IEEE Trans. Automat. Contr.* **2018**, *63*, 2523–2536. [[CrossRef](#)]
54. Gough, J. Principles and applications of quantum control engineering. *Phil. Trans. R. Soc. A* **2012**, *370*, 5241. [[CrossRef](#)]
55. Guo, J.; Chang, J.; Yao, X.; Gröblacher, S. Active-feedback quantum control of an integrated, low-frequency mechanical resonator. *arXiv* **2023**. [[CrossRef](#)]
56. Borah, S.; Sarma, B.; Kewming, M.; Milburn, G. J.; Twamley, J. Measurement-based feedback quantum control with deep reinforcement learning for a double-well nonlinear potential. *Phys. Rev. Lett.* **2021**, *127*, 190403. PhysRevLett.127.190403. [[CrossRef](#)]
57. Ruskov, R.; Korotkov, A.N. Quantum feedback control of a solid-state qubit. *Phys. Rev. B* **2002**, *66*, 041401. PhysRevB.66.041401. [[CrossRef](#)]
58. Jacobs, K.; Lund, A.P. Feedback control of nonlinear quantum systems: A rule of thumb. *Phys. Rev. Lett.* **2007**, *99*, 020501. [[CrossRef](#)]
59. Fu, S.; Shi, G.; Proutiere, A.; James, M.R. Feedback policies for measurement-based quantum state manipulation. *Phys. Rev. A* **2014**, *90*, 062328. [[CrossRef](#)]
60. Zhang, S.; Martin, L.S.; Whaley, K.B. Locally optimal measurement-based quantum feedback with application to multiqubit entanglement generation. *Phys. Rev. A* **2020**, *102*, 062418. [[CrossRef](#)]
61. Bhandari, B.; Czupryniak, R.; Erdman, P.A.; Jordan, A.N. Measurement-based quantum thermal machines with feedback *Control. Entropy* **2023**, *25*, 204. [[CrossRef](#)] [[PubMed](#)]
62. Khalfin, L.A. On the theory of decay at quasi-stationary state. *Sov. Phys. Dokl.* **1958** *2*, 232.
63. Khalfin, L.A. Contribution to the decay theory of a quasistationary state. *Sov. Phys. JETP* **1958**, *6*, 1053.
64. Misra, B.; Sudarshan, E.C.G. The Zeno’s paradox in quantum theory. *J. Math. Phys.* **1977**, *18*, 756–763. 1.523304. [[CrossRef](#)]
65. Balachandran, A.P.; Roy, S.M. Quantum anti-Zeno paradox. *Phys. Rev. Lett.* **2000**, *84*, 4019–4022. PhysRevLett.84.4019. [[CrossRef](#)]
66. Cook, R. J.; Shore, B. W. Coherent dynamics of N -level atoms and molecules. III. An analytically soluble periodic case. *Phys. Rev. A* **1979**, *20*, 539–544. [[CrossRef](#)]
67. Lai, Y.-Z.; Liang, J.-Q.; Müller-Kirsten, H.J.W.; Zhou, J.-G. Time-dependent quantum systems and the invariant Hermitian operator. *Phys. Rev. A* **1996**, *53*, 3691–3693. [[CrossRef](#)] [[PubMed](#)]
68. Wigner, E. P. *Theory and its Application to the Quantum Mechanics of Atomic Spectra [Gruppentheorie und ihre Anwendungen auf die Quantenmechanik der Atomspektren]*; Braunschweig: Vieweg Verlag, 1951; Griffin, J.J., Group, Translator; Elsevier: Amsterdam, The Netherlands, 1959.
69. Sakurai, J.J. *Modern Quantum Mechanics*; Cambridge University Press: Los Angeles, CA, USA, 1985.
70. Kuprov, I. *Spin: From Basic Symmetries to Quantum Optimal Control*; Springer: Berlin/Heidelberg, Germany, 2023. [[CrossRef](#)]
71. Wu, R.; Pechen, A.; Rabitz, H.; Hsieh, M.; Tsou, B. Control landscapes for observable preparation with open quantum systems. *J. Math. Phys.* **2008**, *49*, 022108. [[CrossRef](#)]

Disclaimer/Publisher’s Note: The statements, opinions and data contained in all publications are solely those of the individual author(s) and contributor(s) and not of MDPI and/or the editor(s). MDPI and/or the editor(s) disclaim responsibility for any injury to people or property resulting from any ideas, methods, instructions or products referred to in the content.